Effect of particle size on the magnetic and transport properties of $La_{0.875}Sr_{0.125}MnO_3$

Anulekha Dutta,* N. Gayathri,† and R. Ranganathan‡
ECMP Division, Saha Institute of Nuclear Physics, 1/AF Bidhan Nagar, Kolkata-700064, India
(Received 27 January 2003; published 29 August 2003)

The magnetic and transport properties of nanocrystalline $La_{0.875}Sr_{0.125}MnO_3$ have been studied. Raw samples, prepared by the sol-gel method, were annealed at different temperatures to produce samples of particle sizes 18 nm, 36 nm, and 50 nm. Unlike bulk and single-crystalline samples of the same composition, magnetization data of the nanoparticle samples show no signature of structural transitions. The effects of particle size on the magnetic and transport properties have been attributed to the domain status, changes in the Mn-O-Mn bond angle, and Mn-O bond length in comparison with bulk samples. Field-cooled hysteresis measurements suggest a cluster glasslike behavior in the nanoparticle samples.

DOI: 10.1103/PhysRevB.68.054432 PACS number(s): 75.47.Lx, 73.63.Bd

I. INTRODUCTION

Manganites having colossal magnetoresistive properties have been the subject of various research activities because of the close interplay between the magnetism and the transport exhibited by these manganites.[1] A number of structural and magnetotransport studies of the polycrystalline, single-crystal, and thin films of the doped manganites show that the ferromagnetic Curie temperature and the metal-semiconductor transition temperature are strongly dependent on the preparation method. Of the various manganese perovskites, the $La_{1-x}Sr_xMnO_3$ system has received a lot of interest because it exhibits the highest T_c among all the doped manganite samples. Over the entire composition range, the system exhibits rich magnetic and electrical phases.[1] At low doping levels ($x<0.2$) the system is a canted antiferromagnetic insulator for $x\leqslant 0.1$, a ferromagnetic insulator for $0.1\leqslant x\leqslant 0.15$, and a ferromagnetic metal for $x \geqslant 0.15$. In the low doped regime of the $La_{1-x}Sr_xMnO_3$ system single crystals and bulk polycrystalline samples have been extensively studied because of the series of structural, magnetic, and electronic phase transitions they undergo as a function of temperature which is also a paradigmatic example of the interplay between carrier, lattice, spin, and orbital degrees of freedom.[2–4] The composition of $La_{0.875}Sr_{0.125}MnO_3$ is in the region of ferromagnetic insulator. Exhaustive studies using single-crystal and bulk polycrystalline samples have been performed on this composition. The $La_{0.875}Sr_{0.125}MnO_3$ single crystal shows a series of structural transitions as a function of temperature.[3–13] The first transition is from the high-temperature rhombohedral phase to an orthorhombic (O) phase at 450 K. The second transition occurs at around 270 K ($T_{OO'}$) which is associated with the O to O′ (the Jahn-Teller distorted orthorhombic phase) transition. This O′ phase distorts to the orthorhombic O″ phase at $T\sim 140$ K ($T_{O'O''}$). At $T\sim 180$ K (T_C) $La_{0.875}Sr_{0.125}MnO_3$ shows a paramagnetic to a ferromagnetic metal (FMM) transition which is associated with a decrease in the resistivity with temperature ($d\rho/dT>0$). As the temperature is lowered the FMM state gives way to a ferromagnetic insulator (FMI) at $T\sim 140$ K, which coincides with the $T_{O'O''}$ structural transition. The magnetization shows a sudden increase at this temperature. Detailed neutron-diffraction and high-energy x-ray-diffraction studies have given evidence of charge ordering at this temperature.[3,10–12] Though there were contradictory reports suggesting that the low-temperature phase be called an orbital ordered phase and not a charge ordered phase,[8,9,13,14] now a consensus has been reached that the phase is a charge ordered (CO) one. Dabrowski *et al.* have done a detailed magnetic, structural, and electronic properties study of $La_{1-x}Sr_xMnO_3$ around the composition $x=0.125$.[15] They have observed for $x=0.125$ that $T_C\approx 190$ K and there exists a small anomaly at $T\sim 135$ K where magnetization decreases. The resistivity also shows a decrease at T_C and then again an increase below 140 K which coincides with the T_{CO} observed in single crystals. The transition is rather broad because of the polycrystalline nature of the sample. An earlier report on a similar composition but with a varying oxygen content[16] shows an insulating behavior throughout the temperature range and also a very broad ferromagnetic transition with no particular anomalies in the magnetization.

In this study we examine the influence of particle size on this particular composition of the Sr-doped system. It is well known that reduction in particle size has a direct consequence on the electronic and magnetic properties of a system. Some salient features observed as we reduce the particle size of magnetic systems are (i) a decrease and broadening of the ferromagnetic transition temperature T_C, (ii) a decrease in the magnetization in comparison with single-crystal and bulk polycrystalline samples, showing superparamagnetic behavior at very low particle size, (iii) an increase in resistivity, showing insulating properties at very low particle size, and (iv) a higher value of magnetoresistance compared to the bulk samples especially at low temperatures which is attributed to a spin-polarized intergrain tunneling mechanism.[17] These observations can be logically explained by assuming the increase of an insulating grain-boundary contribution as the particle size decreases.[18–20] Formation of grain boundaries causes broken bonds at the surface, which causes a decrease in the magnetization value. The increase in resistivity is a consequence of the broken bonds as well. This is the most general observation in the case of nanoparticles of the manganite system.[18,21] There are a few exceptions to this general rule. A recent report by Fu[22] on the $La_{0.8}Ca_{0.2}MnO_3$

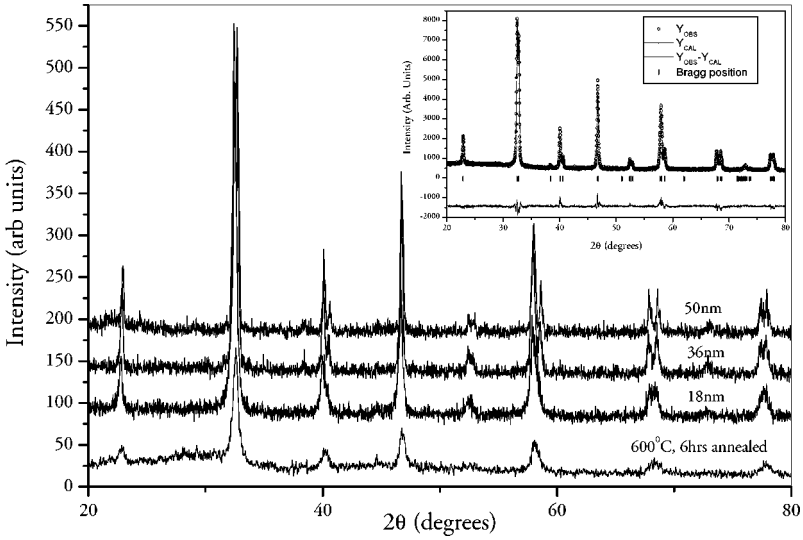

FIG. 1. X-ray-diffraction profiles of the samples annealed for 6 h at 600 °C, 700 °C (18 nm), 900 °C (36 nm), and 1200 °C (50 nm). Inset shows Rietveld refinement profile for the 36-nm sample performed using FULLPROF.

nanoparticle system show results contradicting the above facts on reduced particle size. He has shown that as the particle size decreases, the T_C increases and the resistivity decreases. The decrease in the magnetization with an increase in the particle size and also the increase in the resistivity with the particle size cannot be due to the difference in the oxygen stoichiometry as explained by Fu.[22] The difference has been explained as being due to the strain at the grain boundaries. The deviation from the general rule detailed above seems to be observed with the Sr-doped system as well, especially at low doping. Zhang *et al.* analyzed in detail the effect of the annealing temperature on the magnetization for various x values in the $La_{1-x}Sr_xMnO_3$ system.[23] They found that at low doping ($x<0.25$), the magnetization decreases with an increase in the sintering temperature and for higher doping ($x>0.25$), the magnetization increases with an increase in the sintering temperature. The lattice distortions are mainly responsible for the change of magnetization in this system according to their analysis. In the low doped system of $La_{0.85}Sr_{0.15}MnO_3$, they found that the bond angle decreased and the bond length increased as the sintering temperature increased, which explains the decrease in the magnetization they observed. Our aim in this paper is to study the effect of the particle size on the rich structural, magnetic, and electronic phases exhibited by the $La_{0.875}Sr_{0.125}MnO_3$ system. We have performed a detailed room-temperature structural analysis and taken magnetic and electrical measurements from $T\approx10$ K to 315 K to understand the effect of the particle size on the transitions seen for this composition.

II. EXPERIMENTAL DETAILS

Single-phase, nanocrystalline samples of $La_{0.875}Sr_{0.125}MnO_3$ were synthesized by the sol-gel method. Suitable proportions of La_2O_3, $SrCO_3$, and MnO_2 were used as starting materials. La_2O_3 was prefired at 1000 °C for several hours to decompose residual carbonates. La_2O_3, $SrCO_3$, and MnO_2 were all converted to their corresponding soluble nitrates. La_2O_3 and $SrCO_3$ were readily soluble in dilute nitric acid, however, MnO_2 had to be converted to Mn oxalate first using oxalic acid and then dissolving in dilute nitric acid. The nitrates were mixed in solution, citric acid was added to it, and the resulting solution was slowly evaporated to get a pale orange-colored gel. The gel when decomposed at about 300 °C, resulted in a highly porous black powder. The resulting powder was separated into parts and annealed for 6 h at 600 °C, 700 °C, 900 °C, and 1200 °C to produce samples of different particle sizes. The samples were characterized by x-ray diffraction using a Phillips PW1710-based diffractometer and the particle size was determined independently from x-ray and transmission-electron microscopy (TEM) measurements. The magnetization and hysteresis measurements of the samples were taken with a homemade magnetometer[24] at fields of 10 Oe, 30 Oe, and 60 Oe from $T\approx17$ K to 325 K. The hysteresis measurements were also performed in the same setup. The resistivity was measured by a standard four-probe technique with probes attached using silver paste.

III. RESULTS

A. X-ray diffraction

Room-temperature x-ray-diffraction (XRD) profiles confirmed the pure single phase of the samples at temperatures of 700 °C, 900 °C, and 1200 °C (Fig. 1). The 600 °C sample shows an amorphous background and hence we did not include it in our further studies. The particle sizes as determined from the x-ray data using Scherrer's formula are 18 nm, 36 nm, and 50 nm, for the 700 °C, 900 °C, and 1200 °C annealed samples, respectively. These particle sizes were further confirmed with TEM measurements (Fig. 2). Full profile fitting refinements of the powder-diffraction patterns of all three samples were performed using the program FULLPROF,[25] based on the Rietveld method. We obtained the best fit for the rhombohedral (space group $R\text{-}3C$) structure of the three samples. Our x-ray profiles were modeled using a pseudo-Voigt profile shape function. The refined parameters included the lattice constants, the atom positions, and the occupancy. The detailed values obtained are listed in Table I. Though most of the polycrystalline bulk and single-

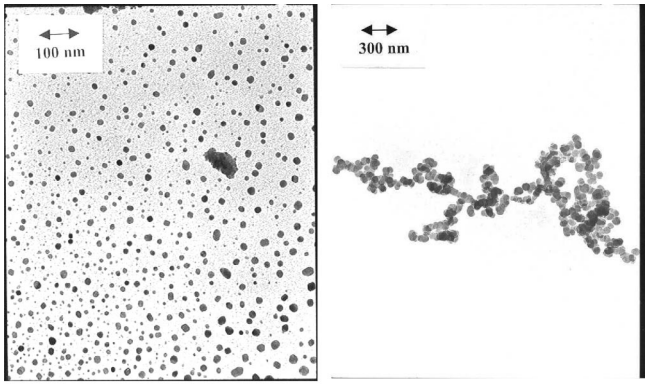

FIG. 2. TEM images of the (a) 18-nm and (b) 50-nm particle size samples.

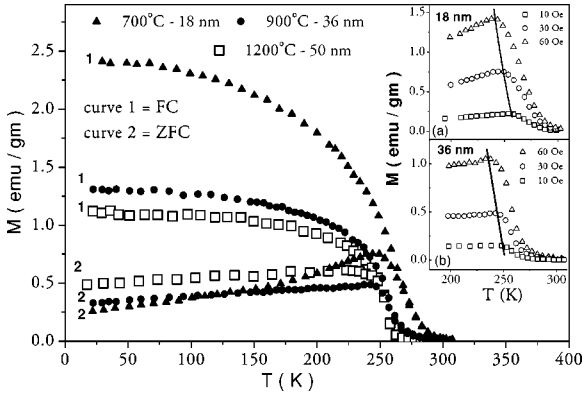

FIG. 3. Magnetization M as a function of temperature measured at H=30 Oe for the three samples. Inset (a) shows $M(T)$ for the 18-nm sample at 10, 30, and 60 Oe. Inset (b) shows $M(T)$ for the 36-nm sample at 10, 30, and 60 Oe. The solid lines are to guide the eye.

crystal samples show a orthorhombic phase at room temperature, there are a few reports on the rhombohedral structure of this composition as well.[2,26] There has also been an report on the stabilization of the high-temperature rhombohedral phase at room temperature for a sample with a very close composition of $x=0.15$.[23] It is well known that the lattice structure of the grain surface is often distorted. This may cause a structural relaxation from the surface to the core of the grain. Since the surface plays a dominant role as the particle size decreases, the internal structure of the grains may be more influenced by the surface for this nanoparticle system. Hence it is possible that we can stabilize a rhombohedral phase at low annealing temperatures for small particle size in these samples. It may be likely that increasing the sintering temperature and time, which promote grain growth, will cause a transition to an orthorhombic structure. This has been observed in the case of the $x=0.15$ sample.[23]

B. Magnetization and hysteresis

The field-cooled (FC) and zero-field-cooled (ZFC) magnetization curves of the three samples measured under a 30-Oe field are shown in Fig. 3. The inset shows M vs T for the 18-nm and the 36-nm samples at three measuring fields. The structural transitions occurring as a function of temperature in this sample composition have been so far reported to be evident in the magnetization plots. However, such signatures are not present in our magnetization data. Detailed low-temperature XRD measurements need to be performed to confirm whether any structural transitions occur in the nanoparticle samples of $La_{0.875}Sr_{0.125}MnO_3$. The T_C values are tabulated in Table II for the three samples. The values are much higher than the reported value of T_C for single-crystal (180 K) (Refs. 4,7,10,11 and 13) and polycrystalline bulk samples (190 K) of the same composition.[15] An interesting feature is that the FC magnetization decreases with an increase in particle size. A large irreversibility between the FC and ZFC curves (which starts at a temperature T_{irr}, tabulated in Table II) is seen for all three samples which suggests the presence of magnetic clusters. The ZFC curve for the 18-nm sample shows a well-defined peak at a temperature $T_P \sim 244$ K (may also be defined as the freezing temperature of the clusters). This ZFC peak is flatter in the 36- and 50-nm cases. Secondly, T_P also shifts with applied magnetic field in these 18-nm and 36-nm samples (as indicated by a line in the inset of Fig. 3) but such a shift is not observed for the 50-nm sample. The magnetization approaching zero as we decrease the temperature and T_P shifting with magnetic field are clear indications of single domain particle behavior. However, the hysteresis behavior of the samples above the freezing temperature T_P confirms that the sample is not superparamagnetic. ZFC and FC hysteresis measurements at different temperatures were taken for all three samples. The ZFC hysteresis loops reproduce the same picture as that of the ZFC magnetization in that the coercive field, h_C, varies with temperature in the same way as does the ZFC magnetization.

TABLE I. List of parameters obtained from the Rietveld analysis assuming a rhombohedral (R-3C) crystal structure.

T_{ann} (°C)	Particle size (nm)	a (Å)	c (Å)	Mn-O-Mn (degrees)	d_{Mn-O} (Å)
700	18	5.4979	13.3435	167.061	1.950(3)
900	36	5.2310	13.3537	165.348	1.960(3)
1200	50	5.5325	13.3616	164.315	1.965(3)
	bulk [a]	5.5246	13.3510	163.87	1.9638(1)

[a]Reference 26.

TABLE II. Tabulation of the various temperatures obtained from the magnetization and resistivity measurements.

Particle size (nm)	T_C (K)	T_P at 30 Oe (K)	T_{irr} at 30 Oe (K)	T_{MI} (K)
18	268	244	269	170
36	257	245	275	170
50	253	224	258	112

However the FC hysteresis curves allow interesting conclusions about the cluster behavior of our samples. We have cooled the sample in the presence of very small fields (H_{FC}) and determined the reverse field (H_C) required to nullify the remanent magnetization produced by the cooling field. The H_C vs H_{FC} data are linear at all temperatures for all samples. dH_C/dH_{FC} (Fig. 4), which is a measure of the cluster response to the magnetic field,[27,32] decreases more sharply with temperature as we decrease the particle size.

C. Resistivity and magnetoresistance

The resistivity of all three samples, without and with a 80-Oe field (Fig. 5), shows two distinct transitions as a function of temperature. As we decrease the temperature the samples show a transition from an insulating to a metallic state at a temperature generally referred to as the metal-insulator transition temperature, T_{MI}. Below $T \sim 51$ K, the samples show an insulating behavior. This temperature may mark the onset of charge and/or orbital ordering in these samples (similar to the case of bulk and single crystals) as is discussed later. We call this temperature T_{CO} (staying with the normal convention followed in this system). The resistivity behavior of the 50-nm sample is quite different from that of the 36-nm and 18-nm samples. The difference between T_{MI} and T_C for this sample is as large as 141 K while it is 86 K and 98 K for the 36 nm and 18 nm samples, respectively. The T_{MI} and T_C for bulk samples coincide. However, T_{CO} does not change for the three samples which indicate that the Mn^{4+}/Mn^{3+} ratio is the same in samples of different particle sizes. This fact confirms that the stoichiometry of the samples are the same, as should be, and that the stoichiometry does not change with annealing temperature. The value of resistivity decreases largely as we decrease the particle size. The MR$[(\rho(H)-\rho(0))/\rho(0)]$ value in a magnetic field as low as 80 Oe is 5% for the 50 nm sample while it is about 3% and 1.5% for the 36 nm and 18 nm samples, respectively, at T_{MI}. The MR as a function of the field is plotted in Fig. 6. It can be seen that the MR behavior for the 50 nm samples is also quite different compared to the 36 nm and 18 nm sample. The MR is highest for the 50 nm sample, and nearly the same for the 36 nm and 18 nm samples (in fields up to 7 kGauss). The low field MR for the 50 nm sample drops sharply with increasing field, whereas the fall is very gradual for the other two samples. This indicates that the grain boundary effects are widely different from the 50 nm sample compared to the 36 nm and 18 nm ones. The MR calculated at 7 T is shown as a function of temperature in the inset of Fig. 6. Two features are clearly observed at high fields. The low temperature transition to the insulating state becomes more broadened, and the MR values of the 18 nm and 36 nm sample (which are almost identical up to 7 kGauss), get quite widely separated out at this high field.

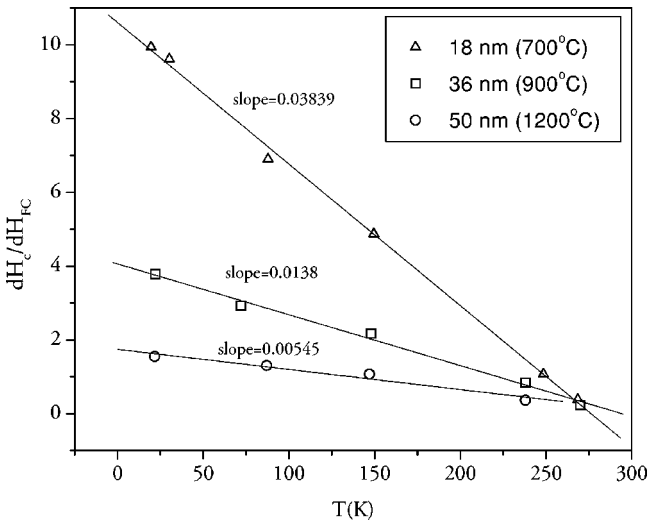

FIG. 4. Plot of dH_C/dH_{FC} as a function of temperature for the three samples.

DISCUSSIONS

Our magnetization data for all three samples show wide ferromagnetic transition. Such wide transition is indicative of a distribution of the strength of exchange coupling arising from weaker magnetic interaction near the grain

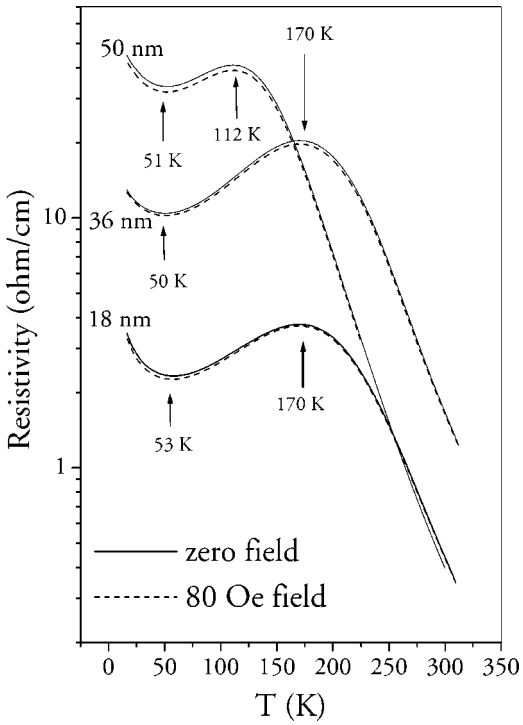

FIG. 5. Resistivity of the three samples as a function of temperature. The dashed lines show the resistivity in an 80-Oe field.

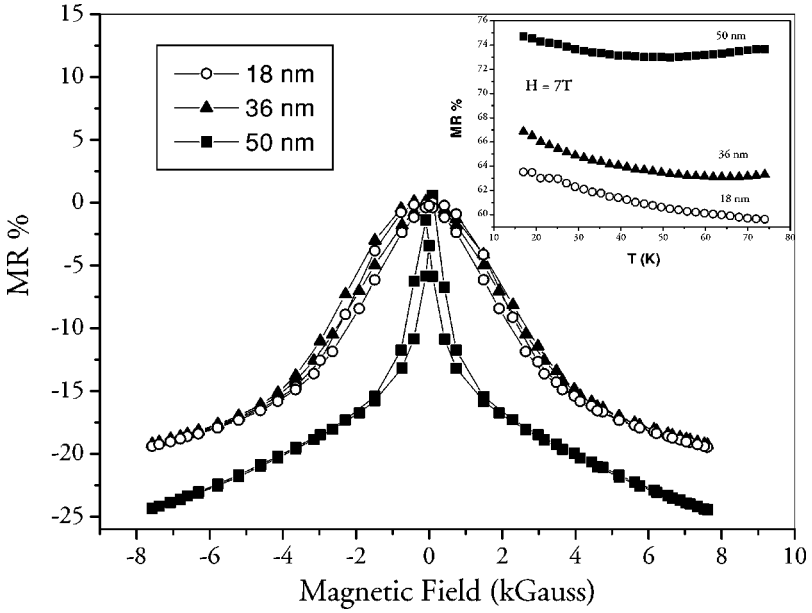

FIG. 6. MR as a function of field for the three samples at $T=77$ K. Inset shows the MR vs T plot for the samples when the applied field is 7 T.

boundary compared to the intragrain contribution, and also due to the distribution of particle size. In our system, TEM pictures show that particle size distribution is quite narrow for the three samples. Hence distribution of the exchange coupling strength seems to play the most important role. The transition hence becomes broad with the decrease of particle size, i.e., with the increase of the grain boundaries. We have estimated the ferromagnetic transition width from the ZFC magnetization data where we define the transition width as the difference between the temperatures at which the magnetization is 90% and 10% of peak value. We find that the widths are 18.5 K, 27 K, 34.5 K for 50 nm, 36 nm, and 18 nm samples, respectively. Short range magnetic cluster formation in the samples results in wide irreversibility between FC and ZFC magnetization. The irreversibility temperature T_{irr} and T_P are magnetic field dependent for 18 nm and 36 nm sample, rather for the 50 nm sample. Interesting conclusions regarding the domain status of the samples can be drawn seeing this field dependence and other features of the ZFC magnetization curves. A cusp in ZFC magnetization is observed in spin glasses as well as in single domain and superparamagnetic particles, although the origin of the behaviour is significantly different for each system. Our sample is not spin glass type because we did not observe any magnetic relazation below T_P. So among the samples, the 18 nm one specially and the 36 nm sample to some extent, can be considered as either single domain or superparamagnetic. If superparamgnetic, then T_P should represent the blocking temperature and above this temperature the sample should not exhibit any hysteresis and also all the magnetization vs H/T curves at different temperatures should collapse into one curve.[28–31] The 18 nm sample does not show any of these two features. We observe a finite width of the hysteresis curve at temperature 270 K (much higher than T_P) and also M vs H/T curves at different temperatures are widely separated. We may conclude that the 18 nm sample is in the single domain regime but it is definitely not superparamagnetic. On the other hand the 50 nm sample shows properties of multidomain particles like a very flattened peak in ZFC magnetization, and T_P not affected by magnetic field. Hence we may say that there is a transition from multidomain to single domain particles when we reduce the particle size from 50 nm to 18 nm. The 36 nm sample nearly marks the transition size because this sample shows features of a mixture of single domain and multidomain particles. The drop in ZFC magnetization below T_P for the 36 nm sample, is not as sharp as the 18 nm one, nor the ZFC peak is as flattened as the 50 nm sample. The shift of T_P with field is less for the 36 nm sample in comparison with the 18 nm one. From the ZFC hysteresis curves at 20 K for all the three samples, we obtain the coercive field h_C, as 6.5 Oe (50 nm sample), 7.2 Oe (36 nm sample), and 5.1 Oe (18 nm sample). The same trend of increase and then decrease in h_C, with decreasing particle size, is obtained at other temperatures. The variation of coercive field with particle size[28,32] should show a peak at the transition from multidomain to single domain. Our h_C variation seems to give a similar picture confirming further the conclusion of transition from multidomain to single domain particles as we decrease particle size from 50 nm to 18 nm. Focusing on the cluster formation in the samples, the FC hysteresis curves give a clear picture. dH_C/dH_{FC} vs T (Fig. 4) plots for different particle sizes is a measure of how the cluster responds to the magnetic field changes with temperature. As we decrease the particle size, the number of clusters in a particle decreases and they become more vulnerable to thermal activation. Hence dH_C/dH_{FC} vs T curve shows a steeper response with changing temperature for the 18 nm sample than the 50 nm one.

The magnetic and transport properites of these perovskite manganites are strongly coupled and are very sensitive to the Mn-O-Mn bond angle and Mn-O bond length. Smaller Mn-O-Mn bond angles, and larger Mn-O bond lengths, tend to reduce magnetization and decrease T_C because the exchange interaction between the Mn ions becomes weaker. The double exchange (DE) model shows that the transfer integral

for electrical conduction between neighboring Mn sites is given by $t = t_0 \cos(\theta/2)$ where θ is the angle between the neighboring Mn spins. It has been found that for fine particle perovskite manganites[18,19,21,33–39] a decrease in magnetization and an increase in resistivity occur as we decrease the particle size, because of broken Mn-O-Mn bonds at the surface of the smaller particles that hamper exchange interaction and degrade connectivity for electron conduction. It is interesting to observe a completely different behavior for fine particle samples of $La_{0.875}Sr_{0.125}MnO_3$. It seems that the spin interaction increases and connectivity improves as we decrease the particle size in this sample. Rietveld analysis of our samples confirms that as we decrease the particle size from 50 nm to 18 nm, the Mn-O-Mn bond angle increases and the Mn-O bond length decreases (Table I). Hence we get increased magnetization and enhanced T_C with decreasing particle size. Bulk sample values of the Mn-O-Mn bond angle and Mn-O bond length are also tabulated in Table I for comparison.

Resistivity as a function of temperature shows two transitions for all three samples similar to the bulk[16,18–21,40] and single-crystal samples.[7–11] As explained in the Introduction, an intermediate metallic behavior $(d\rho/dT > 0)$ occurs between T_C and T_{CO} as seen in the bulk and the polycrystalline samples. But in our samples the transition to the metallic behavior defined as T_{MI} is shifted to a much lower temperature compared to the T_C of the samples. The values of T_{MI} and T_C are listed in Table II as well. It is well known that T_{MI} and T_C are both influenced by the Mn-O-Mn bond angle in these systems. The wide difference between T_C and T_{MI} has been observed earlier in various systems.[36,40,41] In the case of the bulk polycrystalline and single-crystal systems, this deviation has been pointed out as being due to the small A-site cation mismatch in these systems.[40,42] In the case of nanoparticle manganites, a similar deviation of T_C and T_{MI} has been attributed to the effect of the surface strain-induced grain-boundary effects.[21,22] The deviation from ideal oxygen stoichiometry does not generally show such a strong variation of T_C and T_{MI} as explained by Rivas *et al.*[21] Hence the main effect in nanoparticle manganites is due to the grain-boundary effect. Huang *et al.* pointed out that there occur antiferromagnetic insulating regions near the grain boundaries. Such regions do not modify the transition temperature governed by the ferromagnetic core, but can make the electrical transition shift to a low temperature.[41] In our case, this discrepancy between T_{MI} and T_C is an anticipated one, looking at the bond angles and the bond-length variation as a function of the particle size (Table I). The decrease of bond angle and the increase of bond length affects the overlap integral between the two Mn ions and the conductivity between two grains is affected by the grain boundaries as well. The combined effect causes a large difference between T_C and T_{MI} especially as the annealing temperature increases.

The low-temperature transition at T_{CO} to an insulating state in the resistivity plot has been observed in single crystals[7–11] as well as polycrystalline samples[16,18–21,40] of this composition. However one major difference is that this transition is observed at $T \sim 140$ K (T_{CO}) for single crystals and bulk polycrystalline samples while it occurs at about 50 K for all our three samples. This phase is referred to in most cases as the charge/orbital ordered phase. This charge/orbital ordered state is extensively reported to be different from that observed in $LaMnO_3$ in that it is accompanied by an enhancement of a FM state and is hence stabilized by application of external magnetic field. Superexchange (SE) interaction is the origin of ferromagnetism in this phase. Observation of positive magnetoresistance (MR) in the temperature regime just above T_{CO} confirms this charge ordered state.[10,14] In our fine particle samples there is neither an enhancement of magnetization evident in the temperature regime below which an upturn in resistivity occurs, nor does a positive MR appear above it. We in fact get a very broad low-temperature transition which becomes more smeared with the application of magnetic field as high as 7 T, and hence it is difficult to detect any shift in T_{CO} with magnetic field. For polycrystalline samples, along with charge ordering, the grain-boundary contribution results in a small Coulomb barrier of electrostatic origin. This can cause this low-temperature insulating state. Balcells *et al.* and Rivas *et al.* report that an upturn in resistivity occurs for the smallest grains and $\ln \rho$ scales as $1/T^{1/2}$, with the slope giving the grain-size-dependent activation energy.[18,21] Zhu *et al.* reported that the upturn in low temperatures occurs for nanosized particles due to the damage of the double-exchange mechanism in the disordered interfacial region.[19] But then broken surface bonds would also decrease magnetization, and the slope of the $\ln \rho$ vs $1/T^{1/2}$ curve should increase with decreasing particle size. We get just the opposite behavior in magnetization and even though $\ln \rho$ scales very well with $1/T^{1/2}$, there is no change in the Coulomb barrier as a function of particle size. Heilman *et al.* pointed out that Mn-O bond lengths play a crucial role in determining the type of exchange interaction involved.[40] SE interactions, producing an FMI state, involve longer bond lengths than the DE interaction which produces the FMM state. A change in bond length with temperature can result in a transition from one type of interaction to another and consequently give way to the FMM to FMI transition at low temperatures. However, to point out the definite reason for the low-temperature upturn in resistivity for our nanoparticle samples, more extensive investigations need to be done.

Now we focus our attention on the MR in these samples. As pointed out earlier, the general feature of the MR is quite different in the 50-nm sample compared to that of the other smaller particle samples. It has been a general observation that small particles show a higher MR due to the spin-polarized tunneling which has the highest contribution at the lowest temperature. In the manganites, two distinct contributions of MR have been pointed out so far. One is the intrinsic MR which arises due to the suppression of spin fluctuations when the spins are all aligned in the sample on the application of a magnetic field. This MR has the highest value near the ferromagnetic transition temperature and decreases as the temperature decreases. This is generally observed in the case of single-crystal samples and single-crystal thin films. In the polycrystalline samples, there is an additional MR, which is extrinsic in nature, arising due to the intergrain spin-polarized tunneling (ISPT), across the grain boundaries

present in the sample. This MR contribution usually increases as the temperature decreases and also increases as the particle size decreases. Until recently, it was believed that the former mechanism is responsible for the MR at high fields and the latter at low fields. But recent experiments have shown that the high-field response is also due to the existence of the grain boundary, and the nature of the grain boundary is a key ingredient in the mechanism of electric transport, since it constitutes the barriers through which carriers should cross or tunnel.[43,44] In our samples both low-field magnetoresistance (LFMR) and high-field magnetoresistance (HFMR) decreases with decreasing particle size which is in contrast to the behavior observed so far. We get an appreciable MR even at fields as low as 80 Oe. The MR in our samples seems to be an extrinsic type because it appears at the lower-temperature regime and becomes almost negligible at temperatures above T_{MI}. In an 80-Oe field, MR varies from 2% to 5% at T_{CO} and T_{MI}, as we increase the particle size. Rivas *et al.* in fact reported that sol-gel samples sintered at low temperatures show destruction of intrinsic MR.[21] Hence we can say that ISPT is the dominant mechanism for the MR in our samples. But according to the ISPT model, the LFMR should increase with decreasing particle size because we are increasing the disordered surface by decreasing the particle size.[18,19,21] Hence we may have to identify other contributions to the MR by looking at the nature of the field dependence of the MR, which is shown in Fig. 6. From Fig. 6 it is clear that the mechanism of MR is similar in both the 36-nm and 18-nm samples compared to that in the 50-nm sample. To explain this we can take recourse to the domain structure of these samples. The 18-nm and the 36-nm samples are single domain samples, as explained earlier in this section. So application of low magnetic field cannot much improve the intragrain conductivity, hence lower MR percentage values are observed in this case and they almost coincide. The small difference in MR percentage, if it exists at all, between the 18-nm and the 36-nm sample, comes from the distribution of multidomain and single domain particles in the 36-nm sample as it is the transition size from single domain to multidomain. At higher field of 7 T and low temperatures (up to 75 K), the difference in MR percentage between the 18-nm and 36-nm samples increases, as seen in the Fig. 6 inset. This is the effect of better connectivity between grains developed by the high magnetic field in the 36-nm sample. Exchange interaction between grains is already much better for the 18-nm sample compared to the 36-nm sample, so not much difference is a result of the magnetic field. However, for the purely multidomain 50-nm sample a sharp increase in MR percentage is seen when the field is swept from 0 to 1.5 kG (Fig. 6). Fields higher than this affect the intergrain conductivity and this effect is more gradual than affecting the intragrain resistivity, as indicated from the slope of the MR percentage vs H plot in the intergrain region. This slope is also almost identical for all three samples. So we can conclude that in the small particle size range from 18 to 50 nm, ISPT does not change much, but rather it is transition from the multidomain to the single domain structure that plays the major role in the decrease of MR as we decrease the particle size.

IV. CONCLUSION

We have successfully prepared fine particles samples of $La_{0.875}Sr_{0.125}MnO_3$ of 18 nm, 36 nm, and 50 nm by the sol-gel preparation method and studied their low and high magnetic-field response. The sol-gel prepared samples show very different magnetic and transport behavior compared to that of the bulk polycrystalline samples and single crystals of this composition. Determination of the Mn-O-Mn bond angle and Mn-O bond lengths for samples of different particle sizes from Rietveld analysis enables us to explain such contrasting behavior. As the particle size decreases, we see a transition from a multidomain to a single domain regime which brings significant differences in the magnetic-field response of the samples, in terms of magnetization and MR. We are also able to study the cluster response of fine particle $La_{0.875}Sr_{0.125}MnO_3$ from the FC hysteresis measurements. From ZFC hysteresis data at different temperatures we further verify that our 18-nm and 36-nm single domain particles are definitely not superparamagnetic.

*Email address: anulekha@cmp.saha.ernet.in
†Email address: gayathri@cmp.saha.ernet.in
‡Email address: ranga@cmp.saha.ernet.in

[1] *Colossal Magnetoresistive Oxides*, edited by Y. Tokura (Gordon and Breach, New York, 2000); Y. Tokura and Y. Tomioka, J. Magn. Magn. Mater. **200**, 1 (1999); A.P. Ramirez, J. Phys.: Condens. Matter **9**, 8171 (1997); E.L. Nagaev, Phys. Rep. **346**, 387 (2001); Myron B. Salamon and Marcelo Jaime, Rev. Mod. Phys. **73**, 583 (2001).

[2] R.F.C. Marques, M. Jafelicci, Jr., C.O. Paiva-Santos, L.C. Varanda, and R.H.M. Godoi, J. Magn. Magn. Mater. **226-230**, 812 (2001).

[3] J. Nogues, Vassil Skumryev, J.S. Muñoz, B. Martinez, J. Fontcuberta, L. Pinsard, and A. Revcolevschi, Phys. Rev. B **64**, 024434 (2001).

[4] B. Martinez, V. Laukhin, J. Fontcuberta, J. Nogues, V. Skumryev, J.S. Muñoz, L. Pisard, and A. Revcolevschi, J. Appl. Phys. **89**, 6633 (2001).

[5] Vassil Skumryev, J. Nogues, J.S. Muñoz, B. Martinez, R. Senis, J. Fontcuberta, L. Pinsard, A. Revcolevschi, and Y.M. Mukovskii, Phys. Rev. B **62**, 3879 (2000).

[6] H. Kawano, R. Kajimoto, M. Kubota, and H. Yoshizawa, Phys. Rev. B **53**, R14 709 (1996).

[7] L. Pinsard, J. Rodríguez-Carvajal, A.H. Moudden, A. Anane, A. Revcolevschi, and C. Dupas, Physica B **234-236**, 856 (1997).

[8] H. Nojiri, K. Kaneko, M. Motokawa, K. Hirota, Y. Endoh, and K. Takahashi, Phys. Rev. B **60**, 4142 (1999).

[9] Y. Endoh, K. Hirota, S. Ishihara, S. Okamoto, Y. Murakami, A. Nishizawa, T. Fukuda, H. Kimura, H. Nojiri, K. Kaneko, and S. Maekawa, Phys. Rev. Lett. **82**, 4328 (1999).

[10] S. Uhlenbruck, R. Teipen, R. Klingeler, B. Büchner, O. Friedt, and M. Hucker, Phys. Rev. Lett. **82**, 185 (1999).

[11] P. Wagner, I. Gordon, S. Mangin, V.V. Moshchalkov, Y. Bruynseraede, L. Pinsard, and A. Revcolevschi, Phys. Rev. B **61**, 529

(2000).
[12] F. Mayr, C. Hartinger, M. Paraskevopoulos, A. Pimenov, J. Hemberger, A. Lloidl, A.A. Mukhin, and A.M. Balbashov, Phys. Rev. B **62**, 15 673 (2000).
[13] A. Llobet, J.L. García-Muñoz, C. Frontera, M. Respaud, L. Pinsard, A. Revcolevschi, and C. Scott, Physica B **289-290**, 77 (2000).
[14] M. Paraskevopoulos, F. Mayr, J. Hemberger, A. Loidl, R. Heichele, D. Maurer, V. Müller, A.A. Mukhin, and A.M. Balbashov, J. Phys.: Condens. Matter **12**, 3993 (2000).
[15] B. Dabrowski, X. Xiong, Z. Bukowski, R. Dybzinski, P.W. Klamut, J.E. Siewnie, O. Chmaissem, J. Shaffer, C.W. Kimball, J.D. Jorgensen, and S. Short, Phys. Rev. B **60**, 7006 (1999).
[16] D.N. Argyriou, J.F. Mitchell, C.D. Potter, D.G. Hinks, J.D. Jorgensen, and S.D. Bader, Phys. Rev. Lett. **76**, 3826 (1996).
[17] H. Sun and Z.Y. Li, Phys. Rev. B **64**, 224413 (2001).
[18] Ll. Balcells, J. Fontcuberta, B. Martínez, and X. Obradors, Phys. Rev. B **58**, R14 697 (1998).
[19] T. Zhu, B.G. Shen, J.R. Sun, H.W. Zhao, and W.S. Zhan, Appl. Phys. Lett. **78**, 3863 (2001).
[20] Zhi-Hong Wang, Tian-Hao Ji, Yi-Qian Wang, Xin Chen, Run-Wei Li, Jian-Wang Cai, Ji-Rong Sun, and Bao-Gen Shen, J. Appl. Phys. **87**, 5582 (2000).
[21] J. Rivas, L.E. Hueso, A. Fondado, F. Rivadulla, and M.A. Lopez-Quintela, J. Magn. Magn. Mater. **221**, 57 (2000).
[22] Y. Fu, Appl. Phys. Lett. **77**, 118 (2000).
[23] Ning Zhang, Wei Yang, Weiping Ding, Dingyu Xing, and Youwei Du, Solid State Commun. **109**, 537 (1999).
[24] Anindita Ray, A. Chakravarti, and R. Ranganathan, Rev. Sci. Instrum. **67**, 789 (1996).
[25] J. Rodriguez-Carvajal, FULLPROF: *A Program for Rietveld Refinement and Pattern Matching Analysis*, *Abstracts of the Satellite Meeting on Powder Diffraction of the XV Congress of the IUCr*, *Toulouse*, *France*, 1990, p. 127.
[26] J.F. Mitchell, D.N. Argyriou, C.D. Potter, D.G. Hinks, J.D. Jorgensen, and S.D. Bader, Phys. Rev. B **54**, 6172 (1996).
[27] S. Mukherjee, R. Ranganathan, P.S. Anilkumar, and P.A. Joy, Phys. Rev. B **54**, 9267 (1996).
[28] Diandra L. Leslie-Pelecky and Reuben D. Rieke, Chem. Mater. **8**, 1770 (1996).
[29] C.P. Bean and J.D. Livingston, J. Appl. Phys. **33**, 120S (1959).
[30] I.S. Jacobs and C.P. Bean, in *Magnetism*, edited by G.T. Rado and H. Suhl (Academic, New York, 1963), Vol. III, p. 271.
[31] E.P. Wohlfarth, in *Magnetism*, edited by G.T. Rado and H. Suhl (Academic, New York, 1963), Vol. III, p. 351.
[32] Robert C. O'Handley, *Modern Magnetic Materials—Principles and Applications* (Wiley, New York, 2000).
[33] F. Rivadulla, L.E. Hueso, J. Rivas, M.C. Blanco, M.A. Lopez-Quintela, and R.D. Sanchez, J. Magn. Magn. Mater. **203**, 253 (1999).
[34] Huang Yunhui, Yan Chunhua, Wang Zheming, Xu Zhigang, Zhu Tao, Liao Chunsheng, Gao Song, and Xu Guangxian, Sci. China, Ser. B: Chem. **43**, 561 (2000).
[35] Run-Wei Li, Han Xiong, Ji-Rong Sun, Qing-An Li, Zhi-Hong Wang, Jian Zhang, and Bao-Gen Shen, J. Phys.: Condens. Matter **13**, 141 (2001).
[36] Tao Yi, Song Gao, Xing Qi, Yongfa Zhu, Fuxiang Cheng, Baoqing Ma, Yuinhui Huang, Chunsheng Liao, and Chunhua Yan, J. Phys. Chem. Solids **61**, 1407 (2000).
[37] R. Mahesh, R. Mahendiran, A.K. Raychaudhuri, and C.N.R. Rao, Appl. Phys. Lett. **68**, 2291 (1996).
[38] Zhiqiang Jin, Wei Tang, Jianrong Zhang, and Youwei Du, J. Magn. Magn. Mater. **187**, 237 (1998).
[39] M. Respaud, B. Martínez, LI. Balcells, J. Fontcuberta, X. Obradors, J.M. Broto, H. Rakota, and M. Goiran, J. Magn. Magn. Mater. **203**, 100 (1999).
[40] A.K. Heilman, Y.Y. Xue, B. Lorenz, B.J. Campbell, J. Cmaidalka, R.L. Meng, Y.S. Wang, and C. W. Chu, Phys. Rev. B **65**, 214423 (2002).
[41] Yun-Hui Huang, Chun-Hua Yan, Zhe-Ming Wang, Chun-Sheng Liao, and Guang-Xian Xu, Solid State Commun. **118**, 541 (2001).
[42] A. Maignan, C. Martin, G. Van Tendeloo, M. Hervieu, and B. Raveau, Phys. Rev. B **60**, 15 214 (1999).
[43] S. Lee, H.Y. Hwang, Boris I. Shraiman, W.D. Ratcliff II, and S-W. Cheong, Phys. Rev. Lett. **82**, 4508 (1999).
[44] H.Y. Hwang, S-W. Cheong, N.P. Ong, and B. Batlogg, Phys. Rev. Lett. **77**, 2041 (1996).